Heating of Counterstreaming Ion Beams in an External Magnetic Field

K. PAPADOPOULOS, R. C. DAVIDSON,*† J. M. DAWSON,‡ I. HABER, D. A. HAMMER, N. A. KRALL,* AND R. SHANNY

Naval Research Laboratory, Washington, D. C. 20390

(Received 23 June 1970)

Ion heating by a strong ion–ion two-stream instability perpendicular to a magnetic field in the presence of a relatively cold electron background ($T_e \ll m_i V_d^2$) is considered. The magnetic field strength is such that the ion trajectories are straight, whereas the electrons are bound to the field lines ($kr_{Le} \ll 1 \ll kr_{Li}$). Theory is presented for both quasilinear and nonlinear stages of the evolution of the system for the case that the instability is electrostatic [$(B^2/8\pi)\ (1+\beta) > nm_i V_d^2/8$] and is compared with a series of computer simulation experiments. It is found that the quasilinear theory gives a fairly accurate description of spatially averaged plasma properties until the ion beams have been sufficiently modulated for ions to be trapped by the waves. In the subsequent nonlinear stage, stabilization occurs when the ion trapping period is equal to the reciprocal growth rate associated with the instability. The directed ion beam energy is mainly converted into random ion energy. The possible role of this instability in high Mach number shocks is discussed.

I. INTRODUCTION

A strong ion–ion two-stream instability is a possible mechanism that can provide the necessary turbulent dissipation for the formation of collisionless high Mach-number electrostatic shocks.[1] It has been established[2] that in the absence of a magnetic field such an instability is possible under the condition that the electron thermal energy is of the same order as the ion drift kinetic energy. However, the presence of an ambient magnetic field $\mathbf{B}_0$ perpendicular to the streaming motion, with field strength such that the ion motion is not affected by it during the full development of the instability, allows the instability to persist even for negligible electron thermal energy. This is due to the fact that the electrons are tightly bound to the magnetic field lines.

The object of the present paper is to calculate the linear and nonlinear behavior of the ion–ion instability for the case of equidensity ion beams counterstreaming with velocities $\pm\mathbf{V}_d$ perpendicular to $\mathbf{B}_0$ in the presence of a sufficiently cold ($T_e \sim m_e V_d^2$) electron background so that the corresponding $\mathbf{B}_0 = 0$ system would be stable. The results are compared with a series of computer simulation experiments. All variables in the problem are allowed to depend only on the coordinates in the direction of the beam, i.e., the problem is treated essentially as one-dimensional with the perturbation wave vector $\mathbf{k}$ perpendicular to the magnetic field ($\mathbf{k} \perp \mathbf{B}_0$) and along the streaming motion ($\mathbf{k} \parallel \pm\mathbf{V}_d$). However, effects associated with electron drifts in other directions are discussed. In Sec. II the relevant linear, quasilinear, and nonlinear theories are developed in the electrostatic approximation, and the basic conclusions are discussed. In Sec. III we present the results of a series of computer simulation experiments and compare them with the theoretical predictions. Section IV is devoted to a discussion of the validity of the electrostatic approximation, and a brief discussion of the effects of unequal ion beam densities. Finally, in Sec. V we consider the applicability of the strong ion–ion turbulence to high Mach-number shocks.

II. THEORY

The initial velocity space distributions in the x direction are shown in Fig. 1. The ambient magnetic field is in the z direction, and the electron distribution is initially isotropic in the v_x-v_y plane with electron temperature $T_{ex} = T_{ey} = \frac{1}{2} m_e V_d^2$. The counterstreaming ion motion is along the x direction only, and the initial ion temperatures relative to the mean satisfy $T_{ix} = T_{iy} \ll m_i V_d^2$ for each ion beam. The choice of electron temperature is dictated by the stabilization condition of the electron–ion beam instability for initially cold electrons.[3] Since $T_e \ll m_i V_d^2$, the system is stable to the ion–ion two-stream instability in the absence of magnetic field. In relation to the configuration in Fig. 1, consider electrostatic perturbations with electric field $\delta\mathbf{E}$ perpendicular to $\mathbf{B}_0$ and wave vector $\mathbf{k}$ along the x direction. Furthermore, consider the dispersion relation which results from the linearized Vlasov–Poisson equations for the range of parameters

$$k^2 r_{Li}^2 \gg 1, \qquad |\omega|^2 \gg \Omega_{ci}^2, \tag{1}$$

and

$$k^2 r_{Le}^2 \ll 1, \qquad |\omega|^2 \ll \Omega_{ce}^2, \tag{2}$$

where ω is the complex oscillation frequency of the wave, Ω_{ci} (Ω_{ce}) is the ion (electron) gyrofrequency, r_{Le} is the electron thermal gyroradius, and r_{Li} is the effective ion gyroradius (including mean motion). In view of Eq. (1) the ions effectively follow straight line orbits during the time scale of oscillation or growth and are uninfluenced by the presence of the magnetic field to a first approximation. On the other hand, from Eq. (2) the electrons are tightly bound to the field lines with small Larmor radii. Consequently, the appropriate dispersion relation, for electrostatic waves

$$\mathbf{E} = E_0(kx - \omega t)\,\mathbf{k}/|k|$$

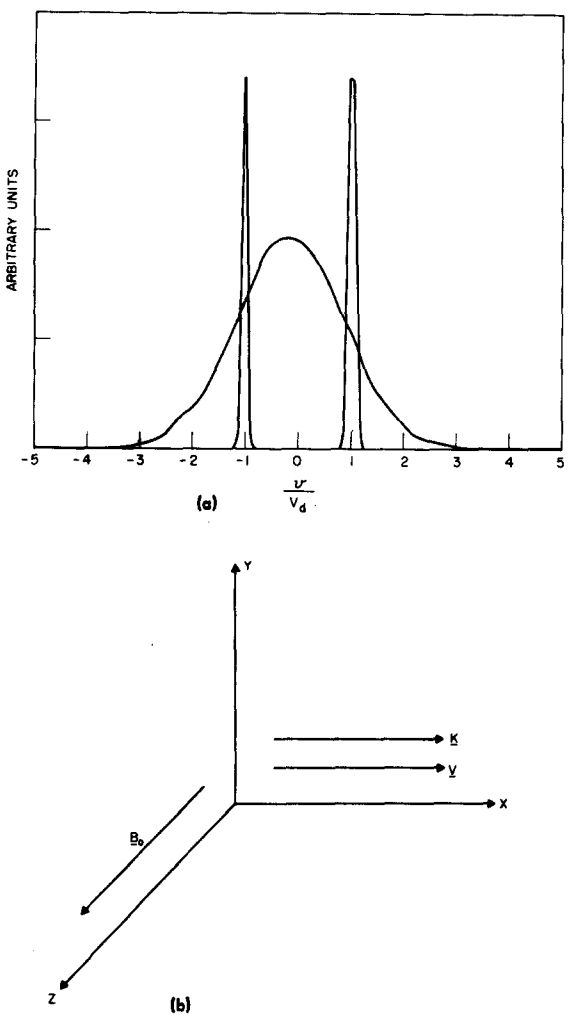

FIG. 1. (a) Initial velocity space of the system. (b) Geometry of the system.

within the context of Eqs. (1) and (2), is given by

$$1+\sum_{j=1,2}\frac{\omega_{pi}^2}{k^2}\int\frac{\mathbf{k}\cdot\partial f_j/\partial\mathbf{V}}{\omega-\mathbf{k}\cdot\mathbf{V}}-\frac{\omega_{pe}^2}{\omega^2-\Omega_{ce}^2}=0. \quad (3)$$

In Eq. (3) ω_{pe} is the electron plasma frequency, ω_{pj} ($j=1, 2$) is the plasma frequency for the jth ion component, and f_j ($j=1, 2$) is the jth component spatially averaged background ion distribution. For the initial configuration shown in Fig. 1 with cold, equidensity, symmetric ion beams, the dispersion relation Eq. (3) takes the form

$$\frac{1}{2}\frac{\omega_{pi}^2}{(\omega-kV_d)^2}+\frac{1}{2}\frac{\omega_{pi}^2}{(\omega+kV_d)^2}=1+\frac{\omega_{pe}^2}{\Omega_{ce}^2} \quad (4)$$

for $|\omega|^2\ll|\Omega_{ce}|^2$. In Eq. (4) $\omega_{pi}^2\equiv 4\pi ne^2/m_i$, where n is the *total* ion background density. The validity of the inequalities in Eqs. (1) and (2) for the unstable solutions to Eq. (4) may be verified *a posteriori*. Defining an effective plasma frequency ω_0, where

$$\omega_0^2\equiv\frac{\omega_{pi}^2/2}{[1+(\omega_{pe}^2/\Omega_{ce}^2)]}, \quad (5)$$

we rewrite Eq. (4) in the familiar form[4] for the symmetric two-stream instability, i.e.,

$$[\omega_0^2/(\omega-kV_d)^2]+[\omega_0^2/(\omega+kV_d)^2]=1. \quad (6)$$

Equation (6) gives instability for wavenumbers in the range

$$0<k^2<k_c^2\equiv 2\omega_0^2/V_d^2. \quad (7)$$

The oscillation frequency $\omega_k=0$ for the unstable waves, and the growth rate γ_k is given by

$$\frac{\gamma_k}{\omega_0}=\left\{\left[\left(1+\frac{k^2V_d^2}{\omega_0^2}\right)^2+\frac{2k^2V_d^2}{\omega_0^2}\left(1-\frac{k^2V_d^2}{2\omega_0^2}\right)\right]^{1/2}-\left(1+\frac{k^2V_d^2}{\omega_0^2}\right)\right\}^{1/2}. \quad (8)$$

The maximum growth rate γ_m occurs for wavenumbers $\pm k_m$ where

$$\gamma_m=\tfrac{1}{2}\omega_0, \quad (9)$$

and

$$k_m^2=\tfrac{3}{4}(\omega_0^2/V_d^2). \quad (10)$$

The inequalities in Eqs. (1) and (2) are trivially satisfied for $k^2=k_m^2$ and $|\omega|^2=|\gamma_m|^2$ provided

$$\Omega_{ce}^2/\omega_{pe}^2\ll m_i/8m_e, \quad (11a)$$

$$m_e v_{e\,\mathrm{th}}^2\ll m_i V_d^2, \quad (11b)$$

where $v_{e\,\mathrm{th}}$ is the electron thermal speed.

Since the beam–plasma system in Fig. 1 is linearly unstable, the perturbations grow exponentially at first and the question arises as to how the system reacts nonlinearly to the unstable field fluctuations.

We now consider the quasilinear evolution of the system during the initial stages of growth before the system becomes highly nonlinear and particle trapping plays a significant role. Useful quantities for present purposes are the mean velocity, $\mathbf{V}_j(t)=\int d\mathbf{v}\mathbf{v}f_j(\mathbf{v}, t)$, and the kinetic energy relative to the mean velocity, $K_j(t)=(m_j/2)\int d\mathbf{v}[\mathbf{v}-\mathbf{V}_j(t)]^2 f_j(\mathbf{v}, t)$, associated with the jth component *spatially averaged* distribution function $f_j(\mathbf{v}, t)$. We closely parallel the analysis of Ref. 3 and take appropriate velocity moments of the quasilinear equation for $f_j(\mathbf{v}, t)$. Therefore, this permits a determination of the momentum loss and heating of the ion beams. For symmetric initial conditions the beam–plasma system in Fig. 1 evolves symmetrically. During the initial stages when the ions have not yet acquired substantial kinetic energy relative to the mean ($K_i\ll m_iV_d^2$), the dispersion relation Eq. (4) holds adiabati-

cally with

$$\frac{1}{2}\frac{\omega_{pi}^2}{[i\gamma_k(t)-kV_i(t)]^2}+\frac{1}{2}\frac{\omega_{pi}^2}{[i\gamma_k(t)+kV_i(t)]^2}=1+\frac{\omega_{pe}^2}{\Omega_{ce}^2} \tag{12}$$

for the unstable waves, and $V_i(t=0)=V_d$. Within the range of validity of Eq. (12), $\gamma_m(t)=\omega_0/2$ and $k_m^2(t)=3\omega_0^2/4V_i^2(t)$. For the present instability the relevant rate equations[3] for each ion component during the initial stages reduce to

$$nm_iV_i(t)\frac{d}{dt}V_i(t)\simeq-3\alpha^2\frac{d}{dt}\epsilon_F(t), \tag{13}$$

$$\tfrac{1}{2}n\frac{d}{dt}K_i(t)\simeq\alpha^2\frac{d}{dt}\epsilon_F(t), \tag{14}$$

where $\epsilon_F(t)=\sum_k|E_k(t)|^2/8\pi$ is the total energy density associated with the unstable electric field fluctuations, and

$$\alpha^2\equiv1+\omega_{pe}^2/\Omega_{ce}^2. \tag{15}$$

Furthermore, the energy density in the unstable field fluctuations grows according to

$$\frac{d}{dt}|E_k|^2=2\gamma_k(t)\,|E_k|^2. \tag{16}$$

Equations (13) and (14) can be written in the convenient dimensionless forms

$$\frac{d}{dt}\left(1-\frac{V_i^2(t)}{V_d^2}\right)\simeq3\alpha^2\frac{d}{dt}\frac{\epsilon_F(t)}{nm_iV_d^2/2} \tag{17}$$

and

$$\frac{d}{dt}\frac{K_i(t)}{m_iV_d^2/2}\simeq2\alpha^2\frac{d}{dt}\frac{\epsilon_F(t)}{nm_iV_d^2/2}, \tag{18}$$

where V_d is the initial ion drift velocity. Equation (17) describes the "slowing down" of each ion beam, whereas Eq. (18) describes the "heating" of each ion component relative to the mean. Since the electrons are in crossed electric and magnetic fields, the kinetic energy $K_{ye}(t)$ associated with their y motion is enhanced by $\mathbf{E}\times\mathbf{B}$ drifts. To the accuracy of Eqs. (17) and (18) this is described by

$$\frac{d}{dt}\frac{K_{ye}(t)}{m_iV_d^2/2}\simeq(\alpha^2-1)\frac{d}{dt}\frac{\epsilon_F(t)}{nm_iV_d^2/2}. \tag{19}$$

Equation (19) may be obtained either from total energy conservation consistent with Eqs. (17) and (18), or by considering the appropriate moment of the quasilinear equation for $f_e(\mathbf{v},t)$. Electron heating in the x direction occurs in higher order than can be calculated accurately from Eqs. (17)–(19). We expect Eqs. (12)–(19) to present a valid description of the evolution of the system as long as the ions are sufficiently cold ($K_i\ll m_iV_d^2$) and particle trapping effects are relatively unimportant. Electron trapping does not play a significant role in the present problem due to their fast Larmor rotation in the v_x-v_y plane. Furthermore, the ions are initially far removed (see Fig. 1) from the phase velocity of the unstable waves since the unstable waves have zero-phase velocity for the symmetric case considered here. Consequently, the time for which Eqs. (12)–(19) are valid may be considerable, i.e., many growth periods. We reiterate that during the initial stages the growth of the electric field is accompanied by a loss in kinetic energy of mean motion for each ion beam, together with an increase in kinetic energy relative to the mean. When the ions become sufficiently hot ($K_i\lesssim m_iV_d^2$), the description by Eqs. (12)–(19) is no longer valid. Even if a quasilinear description were meaningful at this stage it would be necessary, at the very least, to use a more accurate dispersion relation [than Eq. (12)] including ion thermal effects in order to demonstrate actual quenching of the nonresonant ion–ion instability.

However, when the ions become sufficiently hot, ion trapping becomes important. At this stage the electric field has grown to a relatively large amplitude [$\epsilon_F\sim(1/10)nm_iV_d^2/2$ in the simulation experiment] and there are ions moving near the phase velocity of the unstable waves, i.e., some ions are nearly at rest.

With the growth of the potential energy, the ion trapping time

$$\tau_T=(m_i/eE_{\rm rms}k)^{1/2} \tag{20}$$

decreases, and the above theory which is valid for $\gamma\tau_T\gg1$, fails to describe the system correctly. The regime of $\tau_T\sim1/\gamma$ has recently been examined by Manheimer.[5] Assuming particles trapped in a potential wave packet of known statistical properties, he showed that stabilization will occur shortly after the fields reach a level such that

$$\tau_T\sim1/\gamma. \tag{21}$$

At such a field level the wave profile stays constant long enough for the particles to be reflected in the potential well. Subsequently, the field energy can at most grow for a time equal to the reflection time, which will bring complete breakdown of the linear orbit approximation. Therefore, if E_0 is the field given by (20) and (21), the maximum field energy will be

$$\epsilon_{F\,\max}\cong(|E_0|^2/8\pi)\exp[2\gamma(\tau_T/2)]=2.7(|E_0|^2/8\pi). \tag{22}$$

For the instability under consideration Eqs. (9), (10), and (20)–(22) suggest that

$$\frac{\epsilon_{F\,\max}}{\frac{1}{2}nm_iV_d^2}\cong\frac{0.23}{1+(\omega_{pe}^2/\Omega_{ce}^2)}. \tag{23}$$

This estimate is based on a growth rate $\gamma_{\max}$ given by

TABLE I. Summary of computer simulation results. In all cases the total system energy is 100.00.

Experiment No.	Parameters	Time in γ_m^{-1}	Ordered ion energy	Random ion energy	Field energy	Electron energy in X direction	Electron energy in Y direction	Remarks
1	$m_e/m_i=0.04$	0.00	92.48	0.14	0.000	3.69	3.69	
		6.40	16.01	55.00	17.50	3.69	7.80	
	$\omega_{pe}^2/\Omega_{ce}^2=0.25$	10.80	2.75	81.40	6.98	3.70	5.17	
2	$m_e/m_i=0.0025$							
		0.00	99.24	0.26	0.00	0.25	0.25	
		7.70	17.45	60.80	16.95	0.25	4.55	
	$\omega_{pe}^2/\Omega_{ce}^2=0.25$							
3	$m_e/m_i=0.040$	0.00	89.50	3.50	0.00	3.50	3.50	
		6.25	32.46	48.50	6.05	3.65	9.34	
	$\omega_{pe}^2/\Omega_{ce}^2=1.00$	8.00	6.62	78.00	4.45	3.70	7.23	
4	$m_e/m_i=0.010$	0.00	97.33	.82	0.00	1.01	0.94	
		6.75	50.71	32.70	7.22	2.14	8.65	
	$\omega_{pe}^2/\Omega_{ce}^2=1.00$	7.50	21.70	63.20	5.50	2.17	7.53	
5	$m_e/m_i=0.040$	0.00	89.50	3.50	0.00	3.50	3.50	
		6.12	45.38	36.20	1.65	5.56	11.21	
	$\omega_{pe}^2/\Omega_{ce}^2=4.00$	8.70	5.71	73.50	1.60	6.40	12.79	
6	$m_e/m_i=0.040$	0.00	92.51	0.15	0.00	3.67	3.67	Ion-acoustic
		5.80	47.46	32.50	2.44	9.80	17.90	instability
	$\omega_{pe}^2/\Omega_{ce}^2=4.00$	6.45	13.27	55.10	2.70	9.88	19.05	observed first
7	$m_e/m_i=0.040$	0.00	91.75	0.15	0.00	4.00	4.00	Not run to
		4.90	56.68	12.92	0.18	14.40	16.00	completion
	$\omega_{pe}^2/\Omega_{ce}^2=100.00$							

Eq. (9). If, due to electron Landau damping or for any other physical reason neglected in the theory, the actual growth rate is different by a factor λ, that is,

$$\gamma_{\text{act}}=\lambda\gamma_{\max},$$

Eq. (23) should be modified to read

$$\frac{\epsilon_{F\max}}{\frac{1}{2}nm_iV_d^2}=\frac{0.23\lambda^4}{1+(\omega_{pe}^2/\Omega_{ce}^2)}. \tag{24}$$

A notable feature of Eq. (23) is the fact that the ratio of the maximum field energy to the ion drift energy is *independent* of the electron–ion mass ratio and depends only on the ratio $\omega_{pe}^2/\Omega_{ce}^2$.

We also note that the fraction of the total energy which is stored in electron $\mathbf{E}\times\mathbf{B}$ drifts by Eq. (19) plus the electric field energy is constant and independent of the electron–ion mass ratio.

III. COMPUTER EXPERIMENTS

The computer simulation experiments are performed with a one-dimensional *finite size* particle electrostatic code. The code is similar to the one used in Ref. 3 and described in Ref. 6 with the addition of a constant magnetic field perpendicular to the particle motion. The magnetic field is allowed to act only on the electron orbits while the forces on the ions are only due to the self-consistent electrostatic fields in accordance with conditions (1) and (2). Periodic boundary conditions are employed so that a particle leaving one end of the system is reintroduced at the other. For a more detailed technical discussion of the present code and of similar techniques see Ref. 7. In the cases shown below a system containing 2×10^4 electrons and 2×10^4 ions in a grid of 512 points is used. The initial electron and ion velocities were chosen randomly so as to give the following distribution functions:

$$f_e(v)=(\pi V_d^2)^{-1}\exp\left(-\frac{v_x^2+v_y^2}{V_d^2}\right),$$

$$f_i(v)=(\pi v_{i\text{th}}^2)^{-1}\left[\exp\left(-\frac{(v_x-V_d)^2+v_y^2}{v_{i\text{th}}^2}\right)+\exp\left(-\frac{(v_x+V_d)^2+v_y^2}{v_{i\text{th}}^2}\right)\right]$$

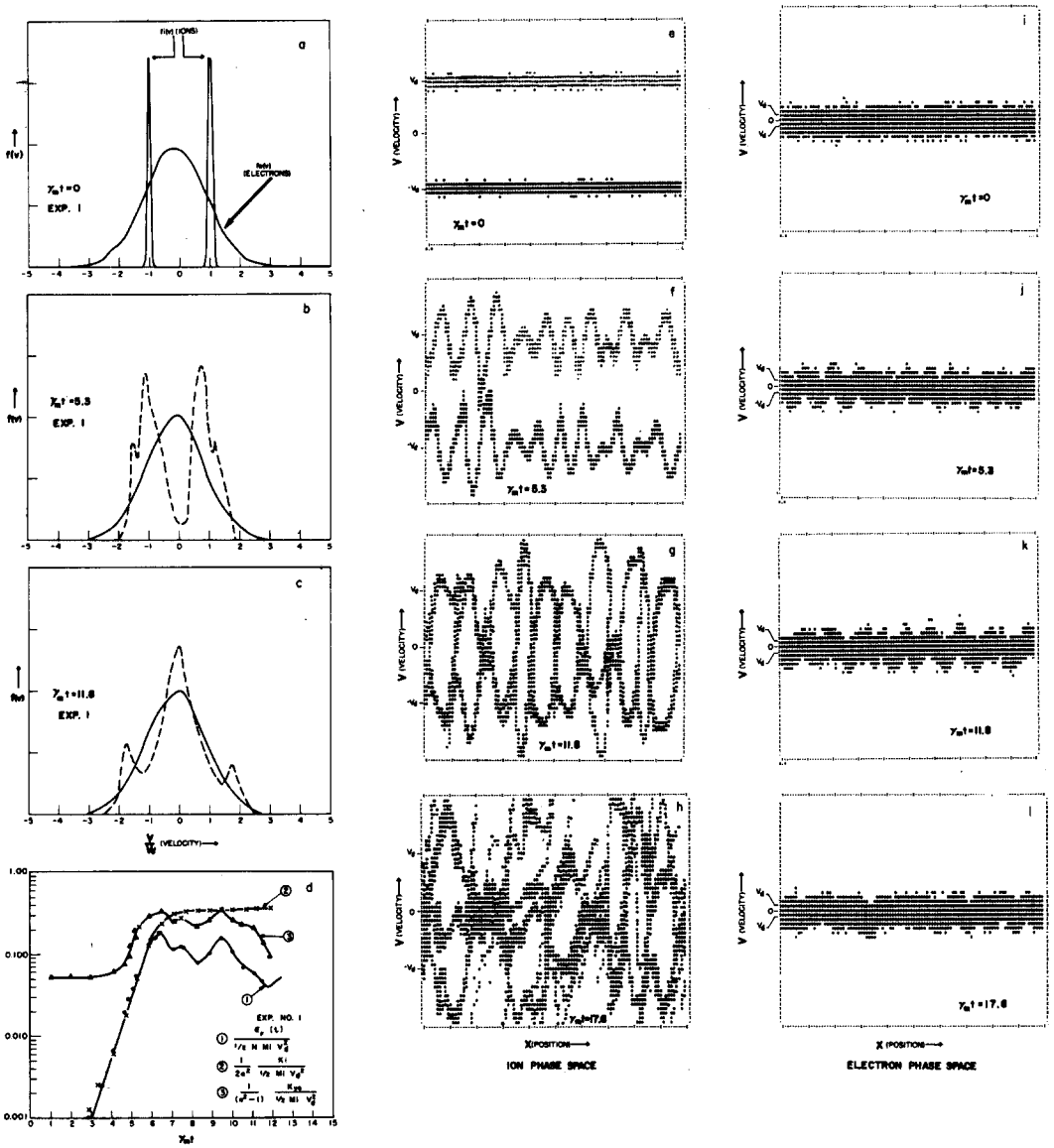

FIG. 2. Results of experiment No. 1. (a)–(c) Electron and ion distribution functions. (d) Time evolution of ϵ_P, K_i, K_{ey}. (e)–(h) Ion (v_x-X) phase space. (i)–(l) Electron (v_y-X) phase space.

with $v_{ith} \ll V_d$. No initial perturbations are introduced beyond the fluctuations inherent in the randomly chosen initial velocities. The time development of the system is followed in phase space and the time development of the relevant quantities is plotted.

A number of different cases are studied by varying the electron to ion mass ratio ($m_e/m_i = 0.0025-0.040$) and the strength of the ambient magnetic field ($\omega_{pe}^2/\Omega_{ce}^2 = 0.25-100$). Table I summarizes the initial experimental conditions and the final stages for each case. Experiment 7 was not carried to completion due to computer time limitation; however, its behavior until the time of its termination was consistent with the conclusions reached from the other experiments and from the theory. Case 6 is similar to case 5, the only difference being in the initial ion temperature (case 6 had $T_i \ll T_e$, case 5 had $T_i \sim T_e$). Since $T_i \ll T_e$, an ion acoustic instability is initially observed. In case 5 since $T_e \sim T_i$, the system was stable with respect to ion acoustic waves. It is found that the behavior of both systems are identical after the ion acoustic instability found in case 6 is stabilized by ion Landau damping.

Figure 2 gives the detailed development of the system for experiment No. 1. The system evolves in a way described by Eqs. (13)–(19) up to time $\gamma_m t \approx 7$. One can see from Fig. 2(c) that at this time some ions have the same velocity as the phase velocity of the waves and can be trapped. The system stabilizes when the field energy ϵ_F reaches the value $\epsilon_{F\,max}$ given by Eq. (22). Care should be exercised in interpreting the results

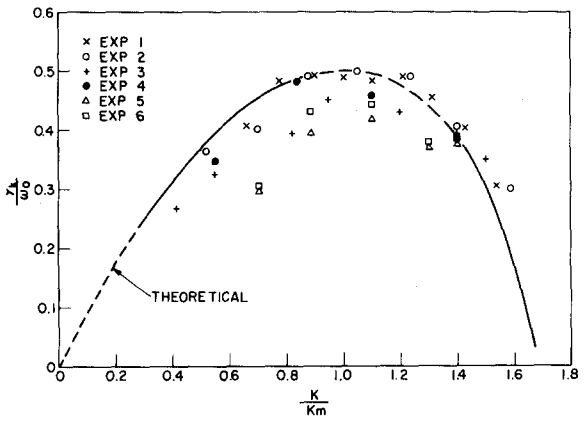

FIG. 3. Growth rate vs wavenumber.

given for $K_{ye}=\frac{1}{2}m_eV_{ey}^2(t)$ and in interpreting the y-electron phase space $(v_y\text{-}x)$. The energy K_{ye} shown in the graphs comes from a completely reversible motion associated with the $[E_x(t)/B_0]c$ drift, and depends linearly on the electric field energy $E_x^2(t)/8\pi$. It is produced by the fact that the simulation does not allow spatial inhomogeneities in the y direction. One can speculate that in a realistic situation the currents associated with the y drifts will result in electron heating in the y direction to an energy $K_{ey}=(\omega_{pe}^2/\Omega_{ce}^2)\epsilon_{F\,\max}$ due to dissipation from the electron–ion drift instability.[8] The results shown in Fig. 2 are typical of the evolutions in phase space observed in all the experiments.

Figure 3 gives the theoretical growth rate vs the wavelength of the instability, Eq. (8), as compared with the value observed in the experiments. One can see that the agreement is excellent for the strong magnetic field cases, but less striking for smaller values of Ω_{ce}/ω_{pe}. This may be related to the fact that the electrons can damp the waves by phase mixing for time intervals of the order $1/\Omega_{ce}$.[9] This does not affect the shape of the $\gamma(k)$ vs k graph (Fig. 3), but it shifts it toward lower values. This shift provides the factor λ of Eq. (24). The fact that electron damping is responsible for the observed lower growth rates in these cases is reflected in the increase of the electron temperature T_{ex} (Table I). Figure 4 shows the time development of the field, the ion random energy, and the ion slowdown for all cases. The smaller growth rates due to electron damping are

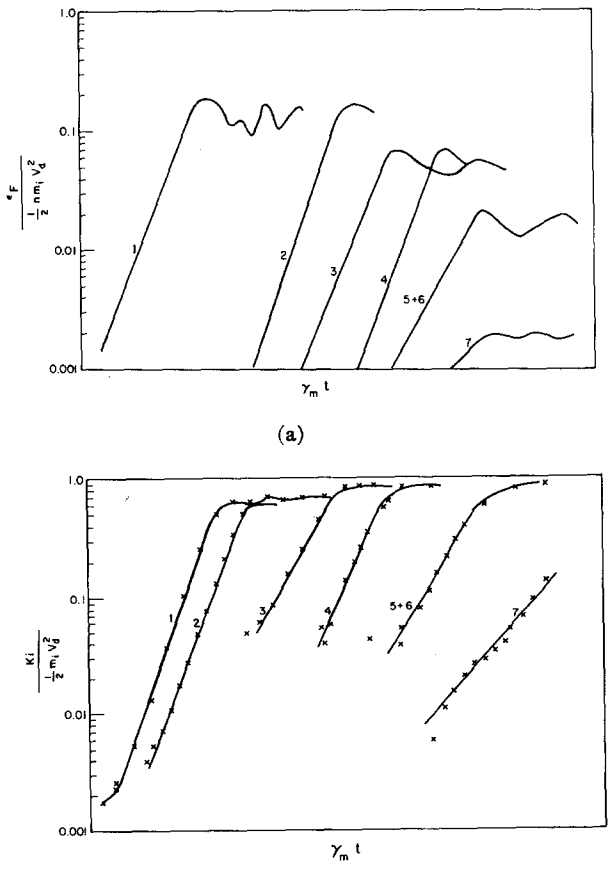

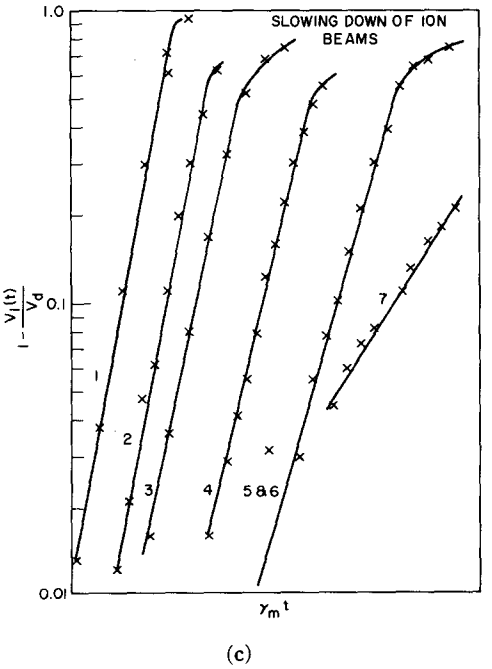

FIG. 4. Results for seven experiments. (a) Time evolution of ϵ_F. (b) Time evolution of K_i. (c) Slowing down of the beams.

responsible for the difference of the slopes of the different runs. Figures 5 and 6 give a comparison of the quasilinear results of Eqs. (16) and (17) with the measured values. The agreement is very good. The nonlinear stabilization level $\epsilon_{F\,\max}$ is shown in Fig. 7. The agreement of the theoretical predictions with the values measured and corrected for the factor λ is also excellent. The factor λ is determined from the shift in the $\gamma(k)$ vs k graph, Fig. 3.

IV. RANGE OF VALIDITY OF THE THEORY

In deriving the results of Sec. II, several assumptions were made. In this section we remark on the conditions of validity of these assumptions. A basic question arises as to when the electrostatic approximation used in Eq. (4) is valid, and whether electromagnetic effects from the finite electron inertia and temperature will stabilize the system. An electromagnetic dispersion relation appropriate to the present problem ($\mathbf{k}$ and $\mathbf{V}_d$ parallel to each other and perpendicular to $\mathbf{B}_0$) can be obtained from the linearized fluid-Maxwell equations.[10,11]

For $\Omega_{ci}\ll kV_d$, ω and $T_i\ll m_iV_d^2$ ion thermal effects and the interaction of the ions with the magnetic field can be neglected. The electron contribution to the dielectric tensor is obtained for isothermal electrons in the low frequency ($|\omega|\ll\Omega_{ce}$), small Larmor radius ($kr_{Le}\ll 1$) limit, keeping the complete interaction of the electron fluid with the electromagnetic field. The resulting dispersion relation is

$$-1+\frac{\omega_{pi}^2}{2(\omega-kV_d)^2}+\frac{\omega_{pi}^2}{2(\omega+kV_d)^2}$$

$$=\frac{\omega_{pe}^2}{\Omega_{ce}^2+k^2v_{e\mathrm{th}}^2-\omega^2}\,\frac{\{k^2-(\omega^2/c^2)+[(\omega_{pe}^2+\omega_{pi}^2)/c^2]\}}{\{k^2-(\omega^2/c^2)+(\omega_{pi}^2/c^2)+[\omega_{pe}^2(\omega^2-k^2v_{e\mathrm{th}}^2)/c^2(\omega^2-\Omega_{ce}^2-k^2v_{e\mathrm{th}}^2)]\}}\,. \quad (25)$$

We wish to ask under what conditions Eq. (25) may reasonably be approximated by Eq. (4) for determining growing modes of the system. One can easily obtain k_c, the marginal stability value of k, by setting $\omega=0$ in Eq. (25). This may be solved for k^2, and written in the form

$$k^2r_{Li}^2=\frac{(1+\beta)}{2[1+\beta+(\Omega_{ce}^2/\omega_{pe}^2)]}\frac{m_i}{m_e}\left\{1-\frac{V_d^2}{V_A^2(1+\beta)}\pm\left[\left(1-\frac{V_d^2}{V_A^2(1+\beta)}\right)^2+\frac{4[1+\beta+(\Omega_{ce}^2/\omega_{pe}^2)]}{(1+\beta)}\frac{V_d^2}{V_A^2}\frac{m_e}{m_i}\right]^{1/2}\right\}, \quad (26)$$

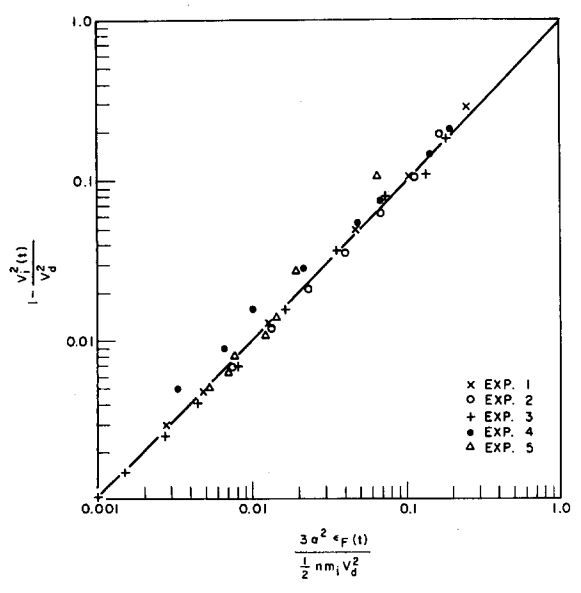

FIG. 5. Comparison of measured ion beam slowing down with quasilinear predictions.

where

$$V_A^2=\frac{B_0^2}{4\pi nm_i}\qquad \beta=\frac{\frac{1}{2}nm_ev_{e\,\mathrm{th}}^2}{B_0^2/8\pi}\,.$$

We take the positive root and impose the constraint $k^2r_{Li}^2\gg 1$ [Eq. (1)]. For $V_d^2/V_A^2(1+\beta)\gg 1$, the right side of Eq. (6) is approximately $1+\beta$; for that parameter equal to 1, it is $\{(1+\beta)m_i/m_e[1+\beta+(\Omega_{ce}^2/\omega_{pe}^2)]\}^{1/2}$; and for $V_d^2/V_A^2(1+\beta)=0$, it is $\{(1+\beta)m_i/m_e[1+\beta+(\Omega_{ce}^2/\omega_{pe}^2)]\}$. For β and $\Omega_{ce}^2/\omega_{pe}^2$ both of order 1 or less, then, we must have

$$V_d^2/V_A^2(1+\beta)<1 \quad (27)$$

in order to be consistent with Eq. (1). In this case, Eq. (4) is a consistent approximation.

Since the local Mach number is $M_A^2=2(V_d/V_A)$, Eq. (27) corresponds to

$$M_A^2(x)<4[1+\beta(x)]. \quad (28)$$

A two-dimensional calculation presently in progress shows that condition (27) is necessary for waves in the whole plane perpendicular to $\mathbf{B}_0$ to be unstable. One can substantially relax it and still have unstable waves over a segment of this plane.

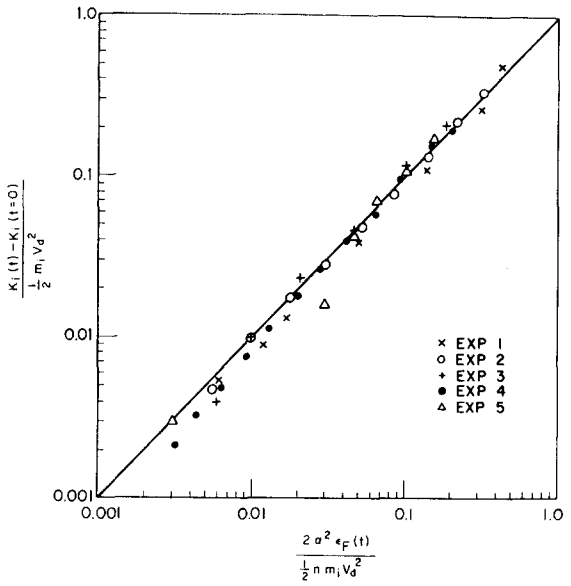

FIG. 6. Comparison of measured ion beam heating rates with quasilinear predictions.

Consequences of the assumptions made along the way were given in relations (1) and (2). The minimum magnitude of $\mathbf{B}_0$ for which this theory is valid must come when electrons can stay in phase with the waves long enough to damp them. This was seen in the computer simulations and was discussed in Sec. III.

If the results of this paper were extended to the case of unequal ion beam densities, the qualitative features

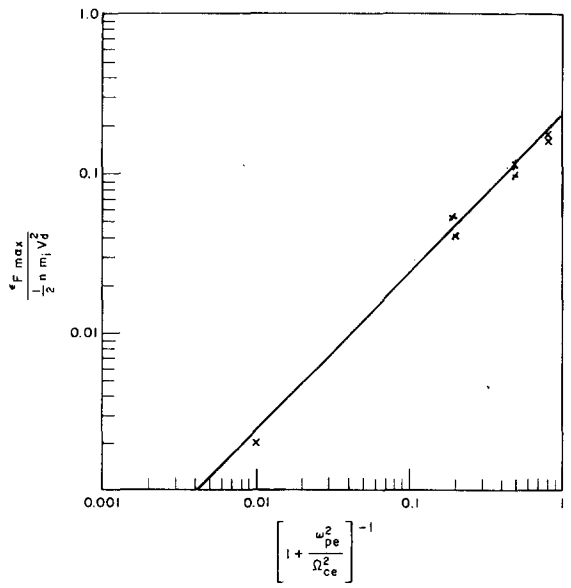

FIG. 7. Field energy at stabilization as a function of magnetic field.

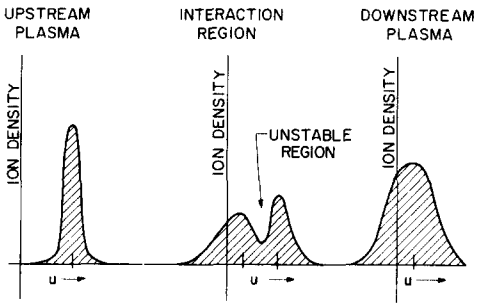

FIG. 8. Proposed high Mach number shock structure.

of the previous two sections would be found to be unchanged. Rates would change, however, since $\gamma_{\max}$ and $k_{\max}$ would be varying with density ratio $\equiv n_1/n_2 \lesssim 1$ according to the approximate relationships

$$\gamma_{\max}/\omega_0 \cong \tfrac{1}{2}[\epsilon^{2/3} + (3^{1/2}/2^{1/3})(\epsilon^{1/3} - \epsilon^{2/3})],$$

$$k_{\max}/\omega_0 V_d \cong \tfrac{1}{2}\{1 + (3^{1/2}-1)\epsilon + [3/4(2)^{1/3}](\epsilon^{2/3} - \epsilon)\}.$$

V. POSSIBLE SHOCK STRUCTURES

It is of interest to see how one can utilize ion–ion interaction provided by this instability in the picture of high Mach number double structure shock waves.[12,13] A proposed structure of such a wave, following Ref. 12, is shown in Fig. 8. A turbulent electrostatic transition is imbedded in an otherwise laminar and slowly varying magnetic shock wave. Table II outlines the three distinct regions of the shock wave. The ion distributions can be of the form shown in Fig. 8. In the interaction region the ion distributions overlap as the upstream plasma mixes with downstream plasma. The presence of the magnetic field allows instabilities of the interacting ion streams as discussed in the earlier section of this paper. The turbulence generated by the instability in the interaction region will be very resistive to particle streaming resulting in hot ions downstream. A more

TABLE II. Shock parameters.

Upstream	Interaction	Downstream
Density $= n_0 < n_f$	Density $= \frac{1}{2}(n_0 + n_f)$	Density $= n_f > n_0$
$\beta < 1$	$\beta \sim 1$	$\beta > 1$
$v_{e\,\mathrm{th}} \sim v_d$	$v_{e\,\mathrm{th}}$ increasing	$\frac{1}{2} m_e v_{e\,\mathrm{th}}^2 < m_i v_d^2$
$v_{i\,\mathrm{th}} \ll V_d$	$v_{i\,\mathrm{th}}$ increasing	
$M_A \gg 1$	$M_A(x) \sim [1+\beta(x)]^{1/2}$	$M_A < 1$

detailed analysis of such high Mach number structures will be given elsewhere.

VI. CONCLUSIONS

We believe that several very instructive results have emerged from the present study. The development of an ion–ion streaming instability in the presence of a strong magnetic field was followed through its early stages until nonlinear saturation. Predictions of the quasilinear moment equations and arguments for nonlinear stabilization by ion trapping were found to agree with the results of the simulation. One can therefore apply, with more confidence, similar simple theoretical considerations in describing more complex systems.

The scaling laws for this particular ion–ion instability were found for a variety of conditions, including the stabilization level of the field fluctuations. Finally, the ion interaction found for distributions of the form in Fig. 8 should be pertinent to the existence of double structure high Mach number shock waves, when the local Mach number falls in the range $M_A^2(x) < 4[1+\beta(x)]$.

* Permanent address: University of Maryland, College Park, Maryland 20742.

† Alfred P. Sloan Research Fellow, 1970-72.

‡ Permanent address: Plasma Physics Laboratory, Princeton University, Princeton, New Jersey 08540.

[1] D. A. Tidman and N. A. Krall, *Shock Waves in Collisionless Plasmas* (Interscience, New York, 1971), Chap. 8.

[2] T. E. Stringer, J. Nucl. Energy Pt. C **6**, 267 (1964).

[3] R. C. Davidson, N. A. Krall, K. Papadopoulos, and R. Shanny, Phys. Rev. Letters **24**, 579 (1970).

[4] O. Buneman, Phys. Rev. **115**, 503 (1959).

[5] W. Manheimer, Phys. Fluids (to be published).

[6] J. M. Dawson, C. G. Hsi, and R. Shanny, in *Plasma Physics and Controlled Nuclear Fusion Research* (International Atomic Energy Agency, Vienna, 1969), Vol. 1, p. 735.

[7] R. L. Morse and C. Nielsen, Phys. Fluids **12**, 2418 (1969). C. K. Birdsall, NASA Report No. SP-153 (1967) and references therein.

[8] J. P. Boris, J. M. Dawson, J. H. Orens, and K. V. Roberts, Phys. Rev. Letters **25**, 706 (1970).

[9] D. G. Baldwin and G. Rowlands, Phys. Fluids **9**, 2444 (1966).

[10] T. Stix, *The Theory of Plasma Waves* (McGraw-Hill, New York, 1962), Chap. 1.

[11] D. W. Ross, Phys. Fluids **13**, 746 (1970).

[12] W. Crevier, Ph.D. thesis, University of Maryland (1969); W. Crevier and D. A. Tidman, Phys. Fluids **13**, 2275 (1970).

[13] A. G. Es'kov, R. Kh. Kurtmulaev, A. I. Malyutiu, V. I. Pil'skii', and V. N. Servenov, Zh. Eksp. Teor. Fiz. **56**, 1480 (1969) [Sov. Phys. JETP **29**, 793 (1969)].

THE PHYSICS OF FLUIDS VOLUME 14, NUMBER 4 APRIL 1971

Resonance Cones in the Field Pattern of a Radio Frequency Probe in a Warm Anisotropic Plasma

R. K. FISHER* AND R. W. GOULD†

California Institute of Technology, Pasadena, California 91109

(Received 29 June 1970)

An experimental and theoretical investigation of the angular distribution of the electric field of a short radio frequency probe in a plasma in a magnetic field is described. The field is observed to become very large along a resonance cone whose axis is parallel to the static magnetic field and whose opening angle is observed to vary with incident probe frequency, cyclotron frequency, and plasma frequency in agreement with simple cold plasma dielectric theory. The relationship of these cones to the limiting phase- and group-velocity cones which appear in the theory of plane wave propagation is discussed. The addition of electron thermal velocities (warm plasma effects) is examined in the limit of a large static magnetic field. A fine structure appears inside the cones and is shown to result from an interference between a fast electromagnetic wave and a slow plasma wave. This interference structure is observed experimentally and measurements of the angular interference spacing are shown to agree with the warm plasma theory. The use of measurements of the resonance cones and structure as a diagnostic tool to determine the plasma density and electron temperature in a plasma in a magnetic field is discussed.

I. INTRODUCTION

The electromagnetic fields and radiation from sources in a plasma in a magnetic field have been the subject of many theoretical studies[1–4] and have become of practical interest in connection with investigations employing rocket and satellite vehicles.

Much of the theoretical interest has centered on the small dipole antenna because of its inherent simplicity. The analysis of an oscillating point dipole in a cold anisotropic plasma[3] shows that the fields should become singular along a cone whose axis is parallel to the static magnetic field and whose opening angle θ_c is determined by the plasma density, magnetic field strength, and incident frequency (see Fig. 1). It has been shown that the Poynting vector is also singular on the resonance cones,[3] so that the total power flow and hence the radiation resistance is infinite for the point dipole antenna. This result, sometimes referred to as the "infinity catastrophe," has stirred considerable controversy.[5] It has been proposed that the inclusion of effects such as electron collisions,[6] electron